An update to this article is included at the end

Engineering Structures 307 (2024) 117891

Contents lists available at ScienceDirect

Engineering Structures

journal homepage: www.elsevier.com/locate/engstruct

Ability of pre-cast strain-hardening cementitious composite plates to enhance the shear performance of RC haunched beams

Mohammed F. Sheta [a,*], Ahmed M. Atta [b], Nesreen Kassem [b], Mahmoud A. Abdel-Aziz [c]

[a] Demonstrator, Structural Engineering Dept., Faculty of Engineering, Tanta University, Tanta, Egypt
[b] Professor, Structural Engineering Dept., Faculty of Engineering, Tanta University, Tanta, Egypt
[c] Assistant Professor, Structural Engineering Dept., Faculty of Engineering, Tanta University, Tanta, Egypt

ARTICLE INFO

Keywords:
RCHBs
SHCC
Strengthening
PSHCC plates
Shear

ABSTRACT

The purpose of this paper is to test ten identical reinforced concrete haunched beams (RCHBs) to determine the effectiveness of pre-cast strain-hardening cementitious composite (PSHCC) plates for shear strengthening. For this purpose, the PSHCC plates have been manufactured in accordance with the test parameters, let to cure for roughly 30 days, and then dipped into the strengthened RCHBs' concrete cover at the critical shear span. The used PSHCC plates are rectangular in shape with a 20 mm thickness and a 100 mm width, and they are reinforced with a single layer of steel wire mesh. The considered key parameters were the effect of shear reinforcement in the test region, the PSHCC plate orientation angle (45^0, 60^0, or 90^0), and the spacing between PSHCC plates (200, 250, or 300 mm). In addition, it was interesting to observe how the strengthening plates, if they exist, are positioned in relation to the inner stirrups (aligned, un-aligned, or inclined). The application of PSHCC substantially enhanced the ultimate shear capacity of the strengthened beams, according to the results of experimental tests. Moreover, the inclined configuration of the PSHCC demonstrated higher shear performance than the vertical configuration, both in terms of the shear cracks characteristics and ultimate capacity. As well, the ductility and serviceability characteristics of the strengthened RCHBs were obviously affected by the application of PSHCC plates. Finally, a proposed analytical model was developed to estimate the shear capacity of the strengthened RCHBs using PSHCC plates.

1. Introduction

RCHBs are structural members described by having a variable depth in relation to their span. Due to their numerous applications, haunched beams are regarded as one of the essential components of construction. Because they simplify the process of positioning equipment items or various facilities, RCHBs have been commonly used in high-rise buildings. Moreover, RCHBs have beneficial applications in bridges and industrial buildings. Strengthening structural components of bridges and industrial structures has become increasingly important [1,2]. In order to avoid interruptions in the building's production, strengthening industrial buildings is preferred to re-construction. Therefore, a significant obstacle now is the need to strengthen RCHBs. There are various studies on the increase of shear load capacity using SHCC to strengthen reinforced concrete prismatic beams [3–6]. On the other hand, the use of SHCC to strengthen RCHBs is not well known.

Regrettably, there aren't any particular recommendations for the strengthening of RCHBs in the United States (ACI 318–19) [7]. Very little information has been published about RCHBs strengthening using other techniques other than SHCC [8–13]. Aziz et al. [9] investigated the behaviour of one prismatic beam and five RCHBs. The quantity of shear reinforcement, the test beams' shape, and the strengthening using CFRP strips were the study's variables. The authors concluded that the shear capacity of tapered beams was raised by 30% by strengthening them using CFRP strips. Additionally, compared to tapered beams without shear reinforcement, the load capacities of tapered beams with half-minimum and minimum shear reinforcement improved by 20% and 33%, respectively, according to the ACI-318 code for prismatic beams. Al-Attar et al. [10] examined the experimental behaviour of fourteen self-compacted RCHBs, some of which were reinforced with CFRP strips. Shear-span to effective depth ratio a/d, haunch angle, and the RCHBs' strengthening technique were the variables examined. According to the experiment results, the ultimate capacity of a haunched beam increases by 56% as the angle of the beam reduces, and the corresponding

* Corresponding author.
E-mail address: Mohammed.Sheta@f-eng.tanta.edu.eg (M.F. Sheta).

https://doi.org/10.1016/j.engstruct.2024.117891
Received 26 September 2023; Received in revised form 20 February 2024; Accepted 18 March 2024
Available online 24 March 2024
0141-0296/© 2024 Elsevier Ltd. All rights reserved.

deflection also reduces. Contrarily, the ultimate capacity improved up to 39% with a reduction in deflection when RCHBs were strengthened with CFRP. Six RCHBs were used in an experiment by Tena-Colunga et al. [13], and two prismatic beams were created and tested to fail in shear with fundamental damage restored. A light-gauge steel wiring mesh covered in a 20 mm thick grout was employed as the external beam jacketing method to improve the deformation and loading capacities achieved by the rehabilitated beams compared to the original beams, proving the effectiveness of the external jacketing method.

It's significant to remember that CFRP strips have a number of benefits. The researchers began to find a new strengthening technique to obtain high compatibility with the concrete surface and to bypass the restrictions resulting from CFRP because the externally bonded CFRP failed as a result of debonding. Over the past three decades, reinforced concrete beams have been strengthened by developing a newer fabric-reinforced cementitious matrix (FRCM) layer [14]. There has been a great development in high-performance fiber reinforced cementitious composites (HPFRCC). The stress-strain curves were studied by Naaman and Reinhardt [15] for three specimens: a specimen of plain concrete, a specimen of fiber reinforced concrete (FRC), and a specimen of HPFRCC during the tensile loading test. With conventional plain concrete, a single unstable crack develops into a brittle failure plane. If not, strain softening occurs right away following cracking in fiber-reinforced concrete. After the initial cracking stage, HPFRCC produce a large number of stable thin cracks that are bridged by fibers.

SHCC material is a particular category of HPFRCC with a strain-hardening behavior [16,17]. A newly developed type of fiber-reinforced cementitious composites known as SHCC is composed of short fibers, fly ash, cement, and silica fume [18–23]. SHCC implements fully under shear and compressive stresses, particularly in regards to energy absorption capacity, in addition to having greater resistance to direct-tension stresses [24,25]. SHCC was also considered an excellent and suitable corrosion-protective material for steel reinforcement because of its narrow microcracks, which offer superior resistance to the entrance of chemicals like oxygen, carbon dioxide, and water. Comparing SHCC to the other strengthening materials, the cost is generally substantially cheaper [26].

Currently, SHCC is regarded as a promising composite for usage in various engineering implementations, such as RC beams [3–6], bridge decks [27–29], wind towers [30], and slabs that experience static loading [17,18]. It was discovered that using SHCC as a strengthening material significantly increased both serviceability and strength. A significant decrease in the developing crack width was also achieved. According to Hussein et al. [31], crack localization is postponed when the SHCC layer has steel reinforcement placed inside of it. In addition, the energy absorption and deformability of the strengthened beams were significantly enhanced by using reinforcement inside the SHCC strengthening layer, according to Khalil et al. [32].

The mechanical response and toughness of Engineered Cementitious Composites (ECC) were investigated by Zhang et al. [33] through four-point bending tests. ECC demonstrated superior mechanical response and enhanced toughness compared to traditional concrete, displaying post-peak ductility, multiple cracking, and self-healing capabilities. In addition, Zhang et al. [34] investigated the performance of RC short walls with and without ECC thin layers under cyclic loading. The walls were evaluated for load-carrying capacity, displacement response, and shear behavior. ECC thin layers significantly improved the cyclic response, increasing load-carrying capacity and enhancing energy dissipation. In general, ECC's crack bridging and self-healing properties contributed to shear force redistribution and prevented further deterioration under cyclic loading.

The literature determined that SHCC is an eminent strengthening material, as demonstrated above. Unfortunately, investigations on its use in strengthening RCHBs are lacking. Determining how haunched beams strengthened with reinforced pre-cast SHCC plates perform structurally in the critical shear span is the aim of the current research. The effects of PSHCC plate orientation angle and the spacing between PSHCC plates were investigated. In addition, the position of the strengthening plates in relation to the inner stirrups was investigated. Finally, to forecast the shear strength of RC haunched beams strengthened using pre-cast SHCC plates, a proposed analytical model was developed.

2. Experimental work program

2.1. Tested haunched beams

The experimental work included ten RCHBs divided into four groups. PSHCC plates were used to strengthen eight beams in the critical shear span. However, the other two beams were kept un-strengthened. With an effective spacing of L = 2800 mm between the supports and a width of 200 mm, all beams were four-point monotonically loaded. The haunched length at both beam ends was 900 mm, which was one-third of the beam's effective span, and the considered angle of slope of the haunch from horizontal (or haunched angle, α) was 9.46°. The linear tapering for each tested beam was carried out by maintaining a constant depth h_{max} = 450 mm at the beam ends while changing the depth of the beam (h_{min}) to 300 mm at the central third with a constant shear span-to-effective depth ratio (a/d_{min}) ≈ 4.2. All beams' geometry satisfies the NTCC-04 standard's criteria for slender beams, which is $L/h_{max} > 5.0$ [35]. Moreover, all beams satisfied the requirement of $a/d_{min} > 2.5$ [36] in order to prevent amplification of the characteristic arching mechanism previously found experimentally in RCHBs [36–41]. For all RCHBs, concrete covers on the sides and vertically maintained at 20 mm.

The studied RCHBs' concrete dimensions and reinforcement details were depicted as shown in Fig. 1. All beams were designed to avoid flexure failure according to ACI 318–19 [7]. In order to achieve this purpose, the compressive reinforcement included 4 bars of 16 mm diameter and 8 bars of 16 mm diameter for the tension longitudinal reinforcement. Finally, shear reinforcement smooth bars spaced 200 mm apart and 8 mm in diameter is used in the test region in four beams and is not used for the remaining beams to clearly determine the impact of the investigated parameters. In contrast, to prevent the occurrence of shear failure outside the measured shear span, the remaining span for all beams was reinforced with stirrups with bars spaced 125 mm apart and 10 mm in diameter.

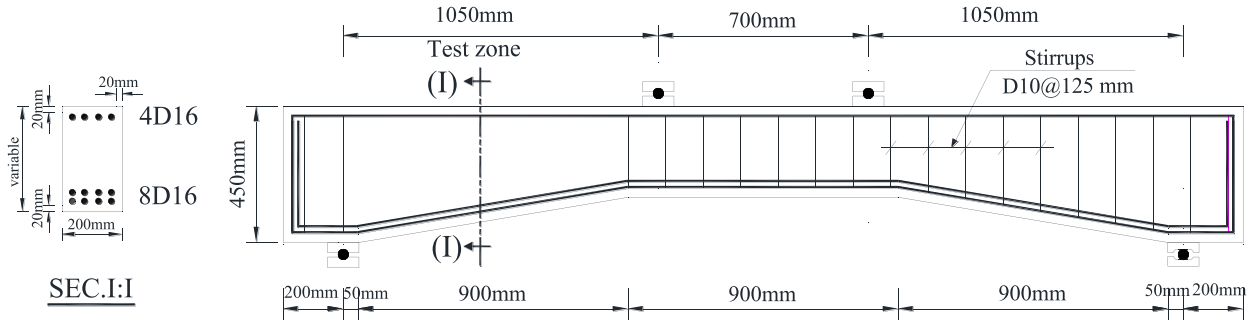
Four test parameters were discussed in this study, as described in Table 1: (a) the effect of shear reinforcement in the test region; (b) the effect of the orientation angle of PSHCC plates; (c) the spacing between the PSHCC plates; and (d) the position of the strengthening plates in relation to the internal stirrups. A schematic illustration of the strengthening system is depicted in Fig. 2.

2.2. Beam nomenclature

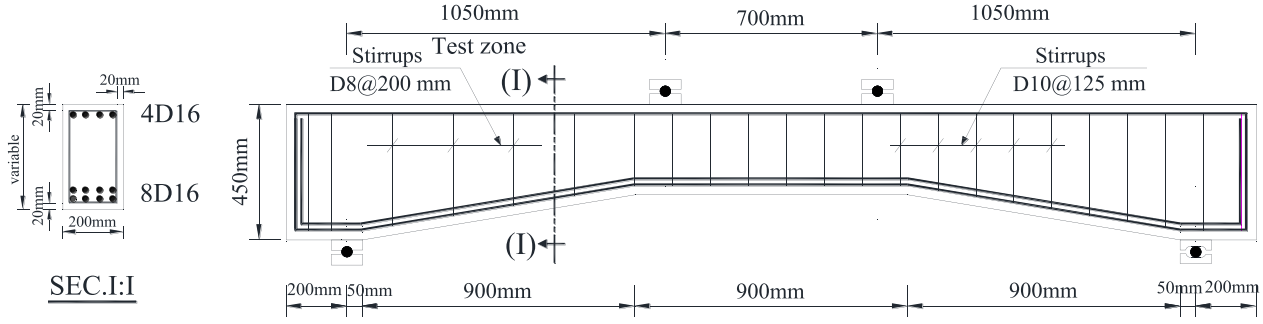
Three subscript symbols separated by a dash are used to identify each strengthened haunched beam. The first symbol denotes the PSHCC plates orientation angle ($\varphi = 45^0, 57^0, 60^0$, and 90^0). The second symbol illustrates the spacing between the PSHCC plates (s_p = 200, 250, and 300 mm). While (NSR or SR) indicates whether or not there is shear reinforcement, this is what the third symbol indicates. The last symbol refers to the position of the SHCC plates relative to the inner stirrups if present in the beam, (Y1 = un-aligned, Y2 = aligned and Y3 = inclined).

2.3. Material properties

To keep the properties of concrete identical in all the reinforced concrete beams used, ready-mixed of normal strength concrete (NSC) was used in casting all the beams. The concrete mixture was made from coarse aggregate with a maximum size of 14 mm, sand, ordinary Portland cement, and water. As a strengthening material, SHCC was utilized. Sand with a diameter less than 0.5 mm, silica fume, water, and ordinary



(a) All beams expect HBC_{SR}, $HBS_{90\text{-}200\text{-}SR\text{-}Y1}$, $HBS_{90\text{-}200\text{-}SR\text{-}Y2}$ and $HBS_{57\text{-}200\text{-}SR\text{-}Y3}$.



(b) Beams HBC_{SR}, $HBS_{90\text{-}200\text{-}SR\text{-}Y1}$, $HBS_{90\text{-}200\text{-}SR\text{-}Y2}$ and $HBS_{57\text{-}200\text{-}SR\text{-}Y3}$.

Fig. 1. The tested haunched beams' concrete dimensions and reinforcement details.

Portland cement, were utilized to develop SHCC, in addition to selecting 1.5% high strength polypropylene (PP) fibers with dimensions of 6 mm in length and 0.012 mm in diameter. The mixtures ratio for both SHCC and NSC are shown in Table 2.

Three standard cylinders with a 150 mm diameter and 300 mm height were used for compression tests on both NSC and SHCC materials according to ASTM C39/C39M-21 [42]. For NSC and SHCC, the average compressive strengths were 24.8 MPa and 59.8 MPa, respectively, at 28 days. A specimen of the SHCC material's compressive stress-strain relationship is shown in Fig. 3. A single layer of steel wire mesh was used to reinforce the PSHCC plates. Steel wire mesh reinforcement was used, with a center-to-center distance of 50 mm and a 2.1 mm wire diameter. Three standard specimens of the used steel wire mesh were subjected to standard tensile tests according to ASTM E8/E8M-22 [43]. The average yield strength was about 235 MPa, and the ultimate strength was around 350 MPa. Additionally, the modulus of elasticity was roughly 201 GPa.

A uniaxial tensile test was conducted on three specimens with a cross section of 50 × 200 mm and a length of 900 mm for each specimen, as shown in Fig. 4, in order to know the tensile properties of SHCC material. The average first cracking strength and ultimate tensile strength of the SHCC specimens were about 4.09 MPa and 7.12 MPa, respectively, as shown in Fig. 5.

RC haunched beams were reinforced in the tension and compression zones using high tensile steel deformed bars that were 16 mm in diameter. All RCHBs were reinforced with 10 mm diameter bars as stirrups along all beams except for the test region. In the test region, smooth bars of normal mild steel with a diameter of 8 mm were used as stirrups. Three specimens of each diameter were subjected to uniaxial tensile tests to investigate the mechanical characteristics of the used reinforcements according to ASTM E8/E8M-22 [43]. Table 3 lists the average mechanical characteristics of the used steel bars. Finally, MasterBrace 1414 epoxy resin locally produced by BASF Company with the mechanical properties shown in Table 4 was used to increase the bonding between the surfaces of the RCHBs and the PSHCC plates. The MasterBrace 1414 epoxy composed of two components A and B mixed thoroughly using a slow speed mixer fitted with a suitable paddle according to the manufacturer's data sheet to obtain a homogeneous mixture.

2.4. Fabrication of the SHCC strengthened beams

All beams were cast in two stages; the PSHCC plates were poured into wooden molds in the first stage. The used PSHCC plates were prismatic plates with a 20 mm × 100 mm rectangular cross-section that were reinforced with steel wire mesh, as illustrated in Fig. 6a. With the suitable dimensions in horizontal wooden formworks, the PSHCC plates were cast. For the PSHCC plates, the wooden molds were filled with the SHCC material, which had a 10 mm thickness (their halves), then steel wire mesh was placed at the intermediate thickness of the PSHCC plates as shown in Fig. 6b. In order to provide the PSHCC plates a total thickness of 20 mm, the mold was filled with the remaining 10 mm of SHCC material, as shown in Fig. 6c. It is significant to mention that the PSHCC plates' upper surfaces were not levelled. It is important for the surface to be rough to ensure proper contact with the epoxy resin (MasterBrace 1414) during bonding of the PSHCC plates to the substrate beam. According to JSCE recommendations [44], all PSHCC plates were demolded after 24 h and then cured by being submerged in water at a temperature of 22 ± 2°C for 30 days to alleviate the issue of the SHCC material's volumetric change.

By the end of 30 days for curing the PSHCC plates, the reinforcing cage of the beams and the SHCC plates were collected together and positioned in the wooden forms to prepare for the second casting stage, as depicted in Fig. 7a through d. The SHCC plate's rough surface was

Table 1
Details of test matrix.

Beam ID	Characteristics	PSHCC plates		The strengthened shear span's stirrups
		φ (degree)	S_p (mm)	
HBC_{NSR}	Control beam in the strengthened shear span without shear reinforcement.	—	—	—
HBC_{SR}	Control beam in the strengthened shear span with shear reinforcement.	—	—	D8 @ 200 mm
$HBS_{45-250-NSR}$	Strengthened beam using inclined PSHCC plates at angle 45°.	45	250	—
$HBS_{60-250-NSR}$	Strengthened beam using inclined PSHCC plates at angle 60°.	60	250	—
$HBS_{90-250-NSR}$	Strengthened beam using vertical PSHCC plates at spacing 250 mm.	90	250	—
$HBS_{90-200-NSR}$	Strengthened beam using vertical PSHCC plates at spacing 200 mm.	90	200	—
$HBS_{90-300-NSR}$	Strengthened beam using vertical PSHCC plates at spacing 300 mm.	90	300	—
$HBS_{90-200-SR-Y1}$	Strengthened beam using PSHCC plates in the strengthened shear span un-aligned with shear reinforcement.	90	200	D8 @ 200 mm
$HBS_{90-200-SR-Y2}$	Strengthened beam using PSHCC plates in the strengthened shear span aligned with shear reinforcement.	90	200	D8 @ 200 mm
$HBS_{57-200-SR-Y3}$	Strengthened beam using PSHCC plates in the strengthened shear span inclined between shear reinforcement.	Variable (average 57)	200	D8 @ 200 mm

PSHCC plates = pre-cast Strain-Hardening Cementitious Composite plates; φ = PSHCC plates orientation angle; S_p = spacing between PSHCC plates; NSR = non shear reinforcement in the test zone; SR = shear reinforcement in the test zone.

placed opposite to the reinforcing cage in order to improve the bond between the pre-cast plates and the concrete core. In addition, the epoxy adhesive layer was applied to the surface of the PSHCC plates until the surface was saturated to a thickness of approximately 2 mm. In the second stage, a ready-mix concrete was used to cast the concrete core. All beams' upper surfaces were cured by wet sackcloth for two weeks, and then allowed to air-drying for another two weeks until the testing day.

2.5. Test setup and instrumentation

The acting load was determined during the force-controlled four-point bending test using a load cell with a capacity of 2000 kN, and it was found that the loading rate ranged for all beams between 0.10 to 0.20 kN/s. In order to determine the produced shear strain, two perpendicular linear variable displacement transducers (LVDTs) were used and placed in the critical shear zone at right angles. LVDTs were used to determine the net mid-span deflection. And for the need to measure the tensile strain, strain gauges were installed on the tensile bars and the stirrups in the critical test zone. An optical microscope was used to determine the width of the critical shear crack. In order to quantify the generated compressive strain in concrete, a PI-shape displacement transducer (PDT) was fixed at the mid-span section of the compression zone. Fig. 8 illustrates the used setup and instrumentation. An automatic data acquisition system was used to collect and store the measured data from PDT, strain gauges, or LVDTs after each loading step.

3. Experimental results and discussion

3.1. Mode of failure

The crack patterns of all tested haunched beams (RCHBs) are depicted in Fig. 9. First, all beams developed flexural cracks in the constant moment area at about 26 kN during the early loading stage. With further loading, the concrete substrate's diagonal shear cracks have begun to spread in the critical shear region. The un-strengthened beam (HBC_{NSR}) recorded the lowest shear cracking load (51 kN). However, using PSHCC plates as a strengthening technique changed the cracking pattern and noticeably improved the cracking load as a result of crack arresting actions and fiber bridging. As a result, the strengthened RCHBs displayed higher cracking loads varied from 9.81% to 19.61% in comparison to beam HBC_{NSR} (see Table 5). The tested beam (whether strengthened or not) experienced shear failure without any yielding of the main tension reinforcements at the final stage of loading.

The apparent failure in the un-strengthened beams (HBC_{NSR} and HBC_{SR}) was with one main crack extending from the point of loading to the support and was inclined with respect to the beam axis. However, the crack distribution was greatly affected by the use of internal stirrups as a shear reinforcement. On the other hand, regardless of the impact of the investigated parameters, all strengthened beams failed owing to concrete splitting together with PSHCC plate rupture characterized by numerous narrower diagonal cracks. It's important to mention that there were no signs of delamination or debonding between the PSHCC plates and the substrate concrete.

As listed in Table 5, cracking loads of beams $HBS_{45–250-NSR}$, $HBS_{60–250-NSR}$, and $HBS_{90–250-NSR}$ were 60, 59, and 57 kN, respectively. The presence of inclined PSHCC plates played an essential role in attempting to control the propagation of cracks as well as improving the ductility of the strengthened beams thereby postponing the brittle shear failure. Additionally, the failure of beam $HBS_{90–300-NSR}$, which developed with a maximum spacing of 300 mm, had two parallel major shear cracks; the first crack extended from the higher mid-point of the critical shear span to the support, While the other crack appeared, extending from the lower mid-point of the critical shear span to the point of loading as depicted in Fig. 9. For instance, the shear cracking load was larger for beam $HBS_{90–200-NSR}$ (61 kN) than that for beam $HBS_{90–250-NSR}$ (57 kN), which in turn exceeded that for beam $HBS_{90–300-NSR}$ (56 kN).

As for the location of the PSHCC plates in relation to the inner stirrups, it is observable that the un-alignment of PSHCC plates with the stirrup legs (beam $HBS_{90–200-SR-Y1}$) demonstrated a larger enhancement in the cracking loads relative to beam $HBS_{90–200-SR-Y2}$ where the PSHCC plates were aligned with the stirrups. As listed in Table 5, the increase in the cracking loads of beams $HBS_{90–200-SR-Y1}$, $HBS_{90–200-SR-Y2}$, and $HBS_{57–200-SR-Y3}$ was 5.08%, 3.38%, and 6.78%, respectively, compared to the beam HBC_{SR}. In contrast to prior beams that failed due to the opening of major shear cracks, both beams ($HBS_{90–200-SR-Y1}$ and $HBS_{90–200-SR-Y2}$) were successful in distributing shear cracks throughout the whole critical shear area resulting in multiples of fine cracks. Generally, strengthening RCHBs in shear using vertical PSHCC plates between the stirrup legs were more efficient than using the PSHCC plates at the same location of the stirrup legs and likewise in the case of using inclined PSHCC plates between shear reinforcement in the test region.

3.2. Ultimate loads

The PSHCC plates, that were used as a strengthening technique, enhanced the ultimate capacity of all tested haunched beams, as listed in Table 5. Based on the investigated parameters, the increase in the

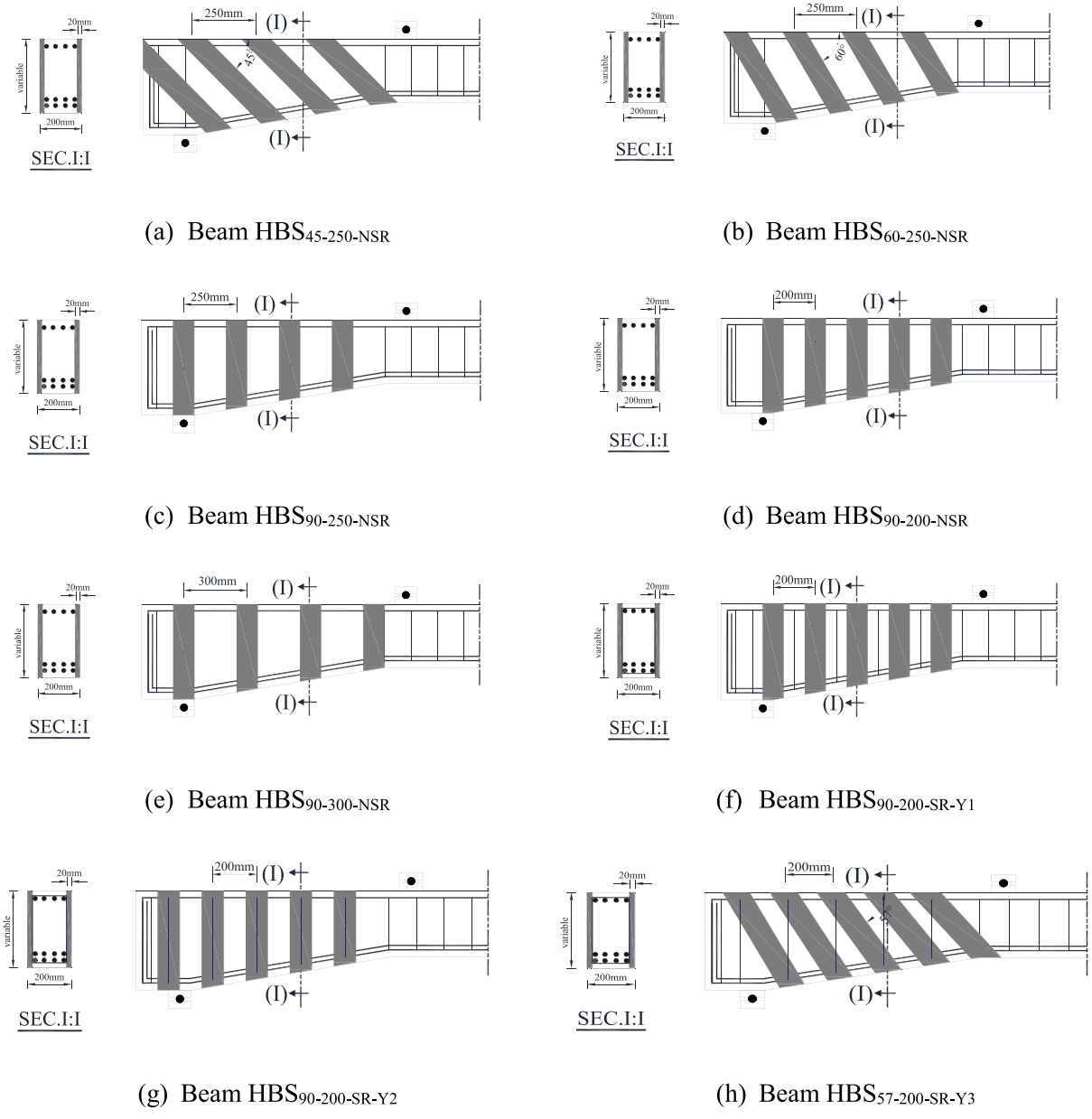


Fig. 2. Scheme of strengthened beams.

Table 2
Mixtures ratio of SHCC and NSC materials per cubic meter (kg/m^3).

Material mix	W/B	Sand	Cement	Water	Coarse pink limestone	Super-plasticizer	PP Fiber (12 mm)	Silica fume
SHCC	0.16	172	1370	270	—	34	16	343
NSC	0.50	545	350	175	1285	—	—	—

SHCC = Strain-Hardening Cementitious Composites; NSC = Normal Strength Concrete; B = cement + silica fume, W/B = water/ binder ratio

ultimate load capacity (P_{exp}) ranged from 81.43% to 144.29% when compared to the un-strengthened haunched beam (HBC_{NSR}). Results for the beams (HBC_{NSR} and HBC_{SR}) indicated that the web reinforcement at the critical shear region within the beam HBC_{SR} significantly increased the ultimate load and significantly delayed cracking relative to the un-reinforced beam HBC_{NSR}, as depicted in Table 5. The experimental results indicated that beams HBC_{NSR} and HBC_{SR} failed at ultimate loads of 70 and 174 kN, respectively.

Regarding the orientation of the PSHCC plates, taking into account the constant plate spacing of 250 mm. The ultimate loads have significantly increased when RCHBs are strengthened with inclined PSHCC plates with orientation angles of 45° and 60° to the horizontal axis of the beam in comparison to 90° (vertical plates). As illustrated in Table 5, beams $HBS_{45–250\text{-}NSR}$, $HBS_{60–250\text{-}NSR}$, and $BS_{90–250\text{-}NSR}$ reached the ultimate loads of 171, 160, and 137 kN, respectively. Of course, the shear capacity is noticeably increased as compared to vertical PSHCC plates

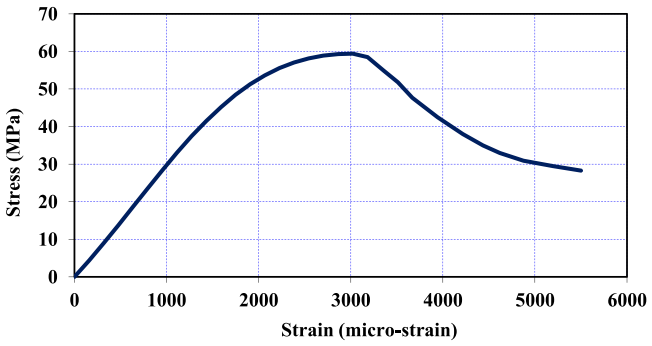


Fig. 3. SHCC specimen's stress-strain during a uniaxial compressive test.

owing to the presence of intermittent inclined strengthening PSHCC plates approximately perpendicular to the primary shear cracks.

Considering the spacing between PSHCC plates, considering the constant plate's orientation of 90°. Comparison between beams $HBS_{90–200\text{-}NSR}$, $HBS_{90–250\text{-}NSR}$, and $HBS_{90–300\text{-}NSR}$ indicated that the spacing between the PSHCC plates significantly affects the ultimate load of the strengthened RCHBs. It is clear that reducing the spacing between plates will lead to an increase in the ultimate capacity. As listed in Table 5, beams $HBS_{90–200\text{-}NSR}$, $HBS_{90–250\text{-}NSR}$, and $HBS_{90–300\text{-}NSR}$ reached the ultimate loads of 162, 137, and 127 kN, respectively. It's important to mention that the suggested small spacing (200 mm) between the PSHCC plates resulted in a significant rise in ultimate shear capacity. The lowest spacing between the PSHCC plates produced the highest increase in shear capacity.

Finally, the location of the strengthening PSHCC plates in relation to the inner stirrups was investigated. The measured capacities were 273, 259, and 282 kN for beams $HBS_{90–200\text{-}SR\text{-}Y1}$, $HBS_{90–200\text{-}SR\text{-}Y2}$, and $HBS_{57–200\text{-}SR\text{-}Y3}$, respectively. These values demonstrate that the strengthened beam using inclined PSHCC plates between web reinforcement in the test region has an average increase in the ultimate load by 62.07% relative to the un-strengthened beam (HBC_{SR}) due to the development of secondary shear cracks in addition to the major one and an increase in the shear capacity detected. In addition, the strengthened beam using vertical PSHCC plates has an average rise in the ultimate load by 56.9% for the beam $HBS_{90–200\text{-}SR\text{-}Y1}$ where the PSHCC plates were un-aligned with the stirrup legs and by 48.85% for the beam whose PSHCC plates aligned with web reinforcement in the test region. This was due to the increase in the contact shear area which has been extended to cover most of the critical shear zone area using inner

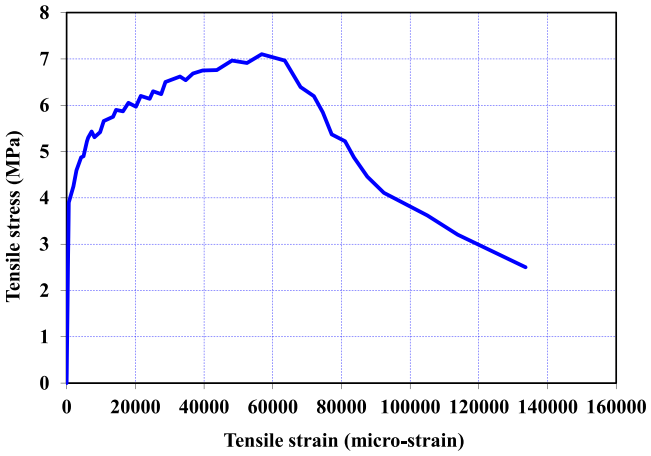


Fig. 5. SHCC specimens' stress-strain plots during a uniaxial tensile test.

Table 3
Summary of characteristics of the used steel material evaluated in lab tests.

Diameter Φ, mm	Yielded strain ε_y (με)	Yielded strength f_y (MPa)	Ultimate strength f_u (MPa)	Young's modulus E_s (GPa)
8	1225	245	375	200
10	2080	420	625	202
16	2065	415	620	201

Table 4
Summary of characteristics of the used mixed resin.

Slant shear bond (MPa)	Tensile strength (MPa)	Compressive strength (MPa)	Bond strength (MPa)
> 11	25	65	> 2.5



Fig. 4. Uniaxial direct tension test of SHCC specimens (All dimensions in mm).

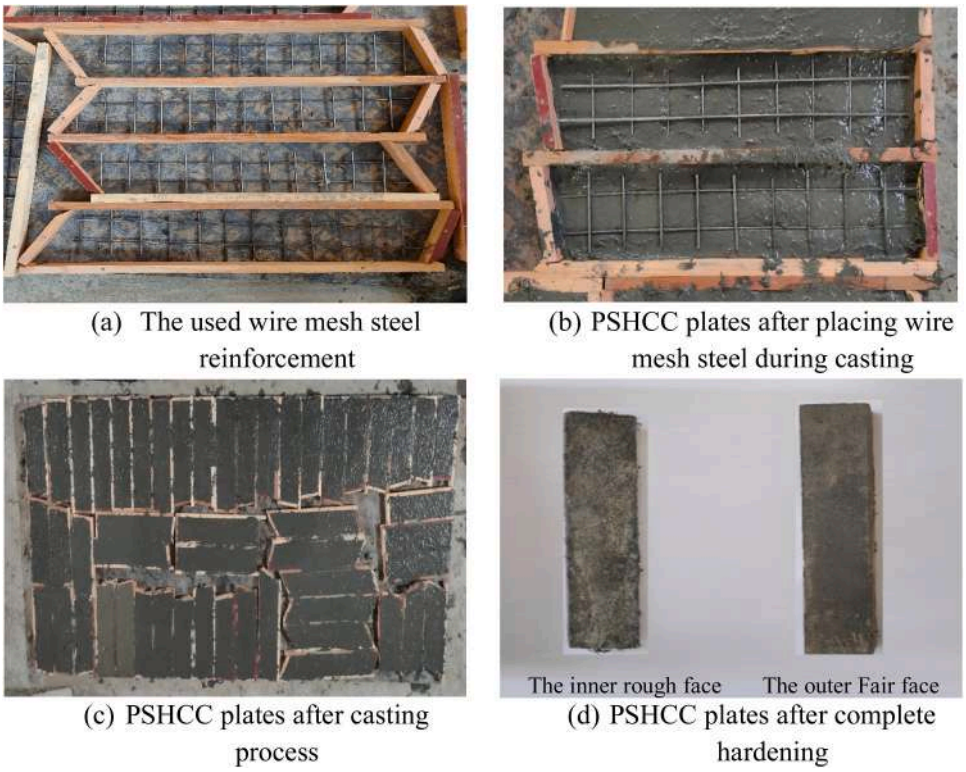


Fig. 6. Fabrication of the PSHCC plates.

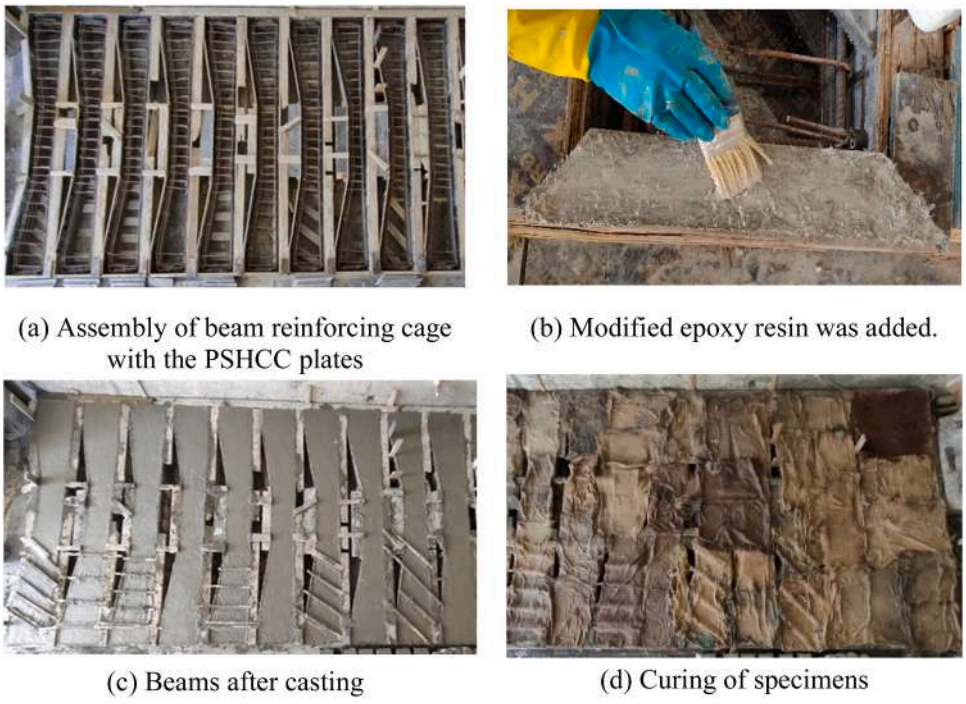
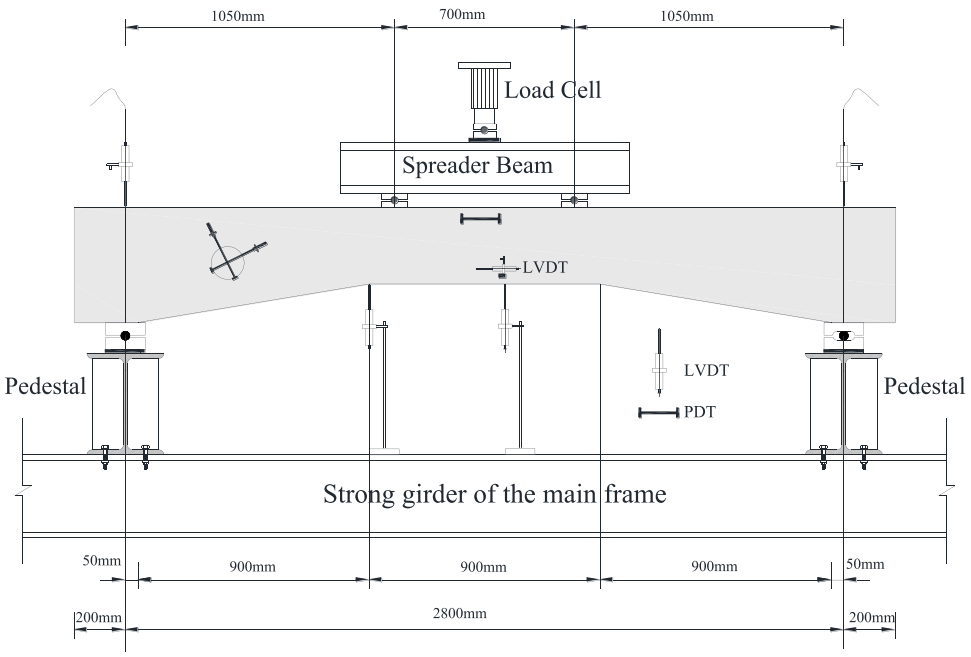


Fig. 7. Fabrication process of test beams.

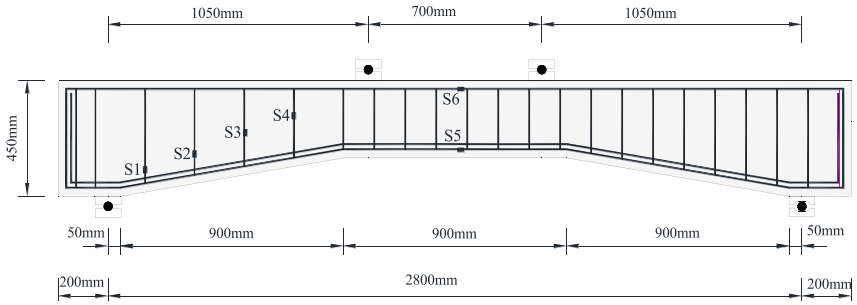
stirrups and the PSHCC plates at different locations rather than confinement of the same points internally by shear reinforcements and externally by the PSHCC plates.

3.3. Load-deflection response

The mid-span net deflection values were recorded for all the tested RCHBs associated with the cracking load, the service load, and the ultimate load (Δ_{cr}, Δ_s, and Δ_u), as indicated in Table 5. The typical load-deflection was illustrated in Fig. 10a to d. It is worth noting that the tested RCHBs showed an almost linear load-deflection response until the relationship became nonlinear, from zero load to 45% of the ultimate load. In general, according to Martínez and Meli [45], the service load was calculated by dividing the ultimate load by a load factor equal to



(a) Four-point loading experiments on RCHBs.



(b) Locations of the applied strain gauges.

Fig. 8. Test setup and instrumentation.

1.5. The un-strengthened beam (HBC_{NSR}) abruptly failed as it reached the ultimate load, and the vertical load reduced quickly. However, depending on the experimental variables, all strengthened beams displayed different post-peak behaviors.

Regarding beams (HBC_{NSR} and HBC_{SR}), results demonstrated that the presence of the web reinforcement at the critical shear zone within beam HBC_{SR} improved initial stiffness (k_i) and ultimate load in comparison to un-strengthened haunched beam HBC_{NSR}, as depicted in Fig. 10a. Table 5 shows that initial stiffness of beam HBC_{SR} was 16 kN/mm with increasing ratio of 14% in comparison to the control beam HBC_{NSR}. It is important to note that the slope of the load-deflection curve was used to determine the initial stiffness of the beam [46]. Briefly, utilization of the inner stirrups as a web reinforcement had a satisfactory influence on initial stiffness and enhanced both the service (Δ_s) and ultimate (Δ_u) deflections versus the unreinforced beam (HBC_{NSR}).

Considering the orientation of the PSHCC plates, changing the orientation angle of the PSHCC plates from 90^0 to 45^0 to the horizontal axis of the beam resulted in an increase in initial stiffness (k_i). Related to the un-strengthened beam (HBC_{NSR}), the initial stiffness of beams $HBS_{90–250\text{-}NSR}$, $HBS_{60–250\text{-}NSR}$, and $HBS_{45–250\text{-}NSR}$ increased by about 10.7%, 14.3%, and 21.4%, respectively (see Table 5). Obviously, the existence of inclined PSHCC plates in strengthening the RCHBs led to a significant improvement in the mid-span deflection response of the tested RCHBs compared to strengthening by using vertical PSHCC plates, as depicted in Fig. 10b.

Pertaining to spacing between the PSHCC plate, comparison between beams $HBS_{90–300\text{-}NSR}$, $HBS_{90–250\text{-}NSR}$, and $HBS_{90–200\text{-}NSR}$ with PSHCC plates of spacing 300, 250, and 200 mm, respectively declared that decreasing the spacing between PSHCC plates had a clear effect on the initial stiffness of the strengthened RCHBs. For particular, the initial stiffness of beams; namely, $HBS_{90–300\text{-}NSR}$, $HBS_{90–250\text{-}NSR}$, and $HBS_{90–200\text{-}NSR}$ were 15, 15.5, and 18 kN/mm, respectively. These values represent an increase of 7.1%, 10.7%, and 28.6%, respectively, relative to the un-strengthened beam (HBC_{NSR}). Finally, a softer post-peak behavior in beams $HBS_{90–300\text{-}NSR}$, $HBS_{90–250\text{-}NSR}$, and $HBS_{90–200\text{-}NSR}$ was obtained as compared to beam HBC_{NSR} (see Fig. 10c).

As for the position of the PSHCC plates in relation to the inner stirrups, beam $HBS_{90–200\text{-}SR\text{-}Y2}$, which was strengthened using PSHCC plates aligned with the stirrup legs, displayed the lowest increased value (18.5 kN/mm) in comparison to the beam (HBC_{NSR}). For in particular, the initial stiffness of beams; namely, $HBS_{90–200\text{-}SR\text{-}Y1}$, $HBS_{90–200\text{-}SR\text{-}Y2}$, and $HBS_{90–200\text{-}SR\text{-}Y3}$ were 19, 18.5, and 19.5 kN/mm, respectively. These values indicate a rise of 18.7%, 15.6%, and 21.9%, respectively, relative to beam HBC_{SR} as listed in Table 5. Finally, beams $HBS_{90–200\text{-}SR\text{-}Y1}$, $HBS_{90–200\text{-}SR\text{-}Y2}$, and $HBS_{90–200\text{-}SR\text{-}Y3}$ showed a softer post-peak behavior versus beam HBC_{SR} (see Fig. 10d). Overall, the ultimate mid-span deflection achieved 18.07 mm for the strengthened beam ($HBS_{45–250\text{-}NSR}$) compared to 7.54 mm for the control beam HBC_{NSR}, a difference of

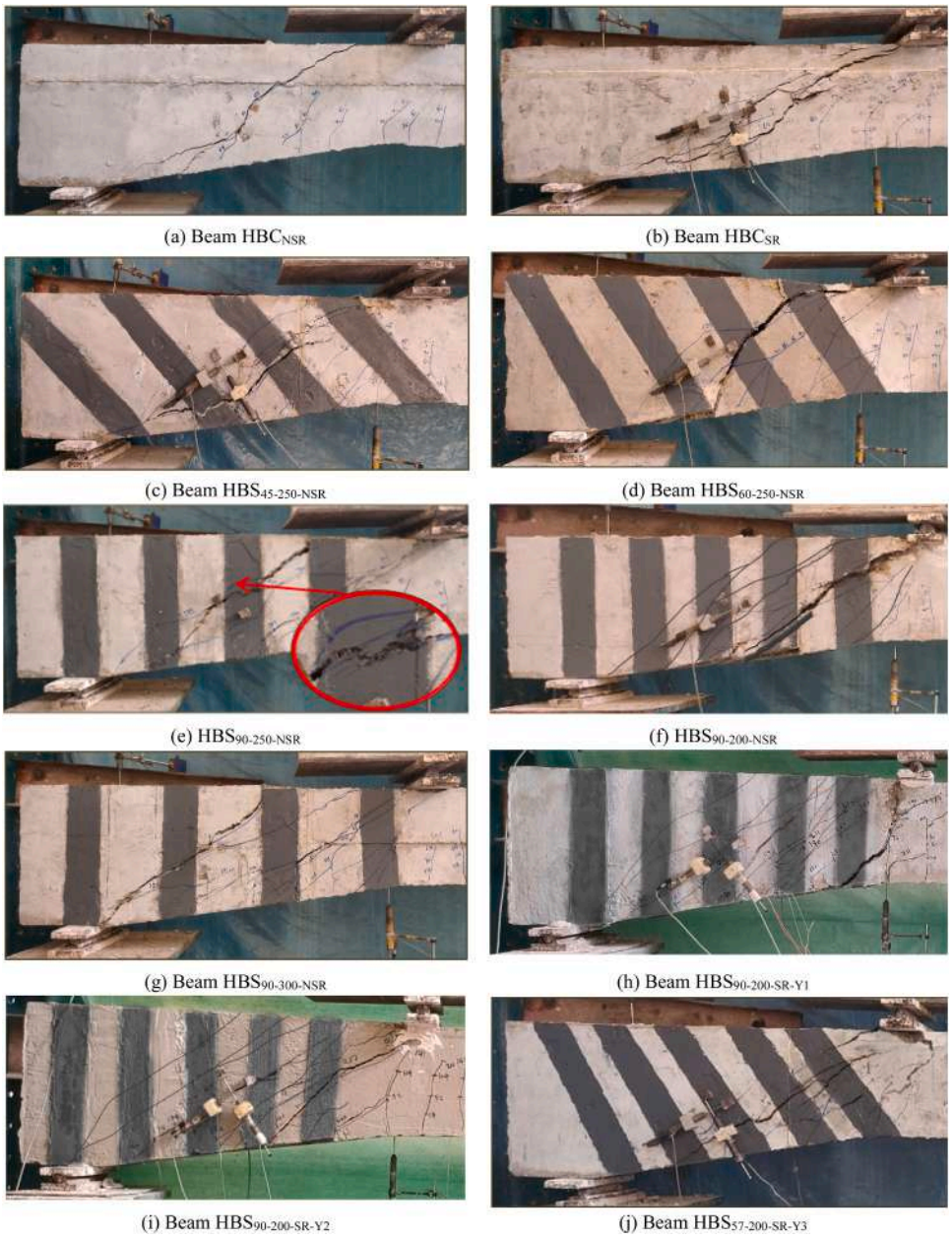


Fig. 9. Failure modes of all tested RCHBs.

139%. This indicates how effectively the pre-cast plates improved the load-deflection response of the RCHBs.

3.4. Energy absorption

Energy absorption (E) is one of the ductility indicators used to ensure that the strengthened beams can withstand large deformations prior to failure and these deformations are inelastic. It is found in the area under the load-deflection curve up to the ultimate point [47]. Among all the beams, the un-strengthened beam (HBC$_{NSR}$) had the lowest energy absorption value (345 kN.mm). However, using the PSHCC plates to strengthen the critical shear span of the tested RCHBs, an improvement in energy absorption of 467% was observed for the strengthened beam (HBS$_{45-250-NSR}$).

The utilization of the inner stirrups as a web reinforcement had an acceptable influence on the crack distribution and enhanced the energy absorption by 5.94 times relative to beam HBC$_{NSR}$. On the other hand, the beams strengthened using inclined PSHCC plates, taking into account the constant plate spacing of 250 mm, showed energy absorption values ranging from 1957 kN.mm (HBS$_{45-250-NSR}$) to 1673 kN.mm (HBS$_{60-250-NSR}$), with an average increase of 426% relative to the un-strengthened beam (HBC$_{NSR}$). Due to the minimization of spacing between PSHCC strengthening plates for beam HBS$_{90-200-NSR}$, the energy absorption value (1415 kN.mm) of the considered beam was significantly higher than other beams (HBS$_{90-250-NSR}$ and HBS$_{90-300-NSR}$). Additionally, RCHBs that had been strengthened with PSHCC plates and web reinforcement at the crucial shear span showed a significant improvement in energy absorption. The energy absorption for the strengthened beams HBS$_{90-200-SR-Y1}$, HBS$_{90-200-SR-Y2}$, and HBS$_{90-200-SR-Y3}$ reached 12.24, 11.41, and 13.02 times, respectively, in relation to the beam HBC$_{NSR}$. This may be explained as; using PSHCC plates and web reinforcement altered the propagation of shear cracks. Overall, according to the previous data, it was clear that adopting PSHCC plates as a strengthening technique led to a superior improvement in the tested RCHBs' ductility behaviour (see Table 5).

Table 5
Test results.

Beam I.D	Loads & Gain in strength				Displacement & Initial stiffness					Energy absorption		Mode of failure		Mode of failure
	P_{cr} (kN)	Gain in P_{cr} (%)	P_{exp} (kN)	Gain in P_{exp} (%)	Δ_{cr} (mm)	Δ_s (mm)	Δ_u (mm)	k_i (kN/mm)	Gain in k_i (%)	E (kN.mm)	E/ E_{HBCNSR}	ε_s	ε_c	
HBC_{NSR}	51	NA	70	NA	3.87	4.84	7.54	14	NA	345	NA	501	1005	Diagonal Splitting
HBC_{SR}	59	15.68	174	148.57	4.15	9.27	18.78	16	14.2	2048	5.94	1063	1662	
$HBS_{45\text{-}250\text{-}NSR}$	60	17.64	171	144.29	3.87	8.88	18.07	17	21.4	1957	5.67	1757	2365	PSHCC plates ruptured in addition to the diagonal splitting.
$HBS_{60\text{-}250\text{-}NSR}$	59	15.68	160	128.57	3.96	8.42	16.91	16	14.3	1673	4.85	1796	2098	
$HBS_{90\text{-}250\text{-}NSR}$	57	11.76	137	95.71	3.89	6.95	13.53	15.5	10.7	1135	3.29	1522	1986	
$HBS_{90\text{-}200\text{-}NSR}$	61	19.61	162	131.43	3.83	8.04	14.67	18	28.6	1415	4.10	1801	2487	
$HBS_{90\text{-}300\text{-}NSR}$	56	9.81	127	81.43	3.76	6.91	13.41	15	7.1	1056	3.06	1377	1790	
$HBS_{90\text{-}200\text{-}SR\text{-}Y1}$	62	5.08 *	273	56.90 *	3.88	14.66	26.25	19	18.7 *	4222	2.06 *	1824	2757	
$HBS_{90\text{-}200\text{-}SR\text{-}Y2}$	61	3.38 *	259	48.85 *	3.78	14.58	25.74	18.5	15.6 *	3935	1.92 *	1659	2588	
$HBS_{57\text{-}200\text{-}SR\text{-}Y3}$	63	6.78 *	282	62.07 *	3.95	14.51	26.77	19.5	21.9 *	4495	2.19 *	1956	2963	

P_{exp} = experimental ultimate load; P_{cr} is the first shear cracking load on the concrete substrate; Δ_{cr} is the first shear cracking load-corresponding deflection at mid-span; Δ_s = the service load's corresponding deflection at mid-span; Δ_u = the failure load's corresponding deflection at mid-span; E = energy absorption; E_{HBCNSR} = energy absorption for the beam (HBC_{NSR}); k_i = initial stiffness; ε_s is the main reinforcement's maximum tensile strain at the mid-span section (με); ε_c is the mid-span section's maximum compressive strain in concrete (με); * The values were evaluated in relation to the beam (HBC_{SR}).

3.5. Cracking evaluation

Referring to Fig. 11a to d, which graphically depict the relationship between the applied load for all tested RCHBs and the major shear crack's width formed on the concrete substrate, provides more information on crack width. The results demonstrated that both RC haunched beams (HBC_{NSR} and HBC_{SR}) exhibited the same behaviour prior to the cracking load. The usage of inner stirrups at the critical shear zone (beam HBC_{SR}) effectively reduced the major shear crack's width compared to beam HBC_{NSR} once the cracking loads were reached. At about 66 kN, the measured width of the shear crack for beams HBC_{NSR} and HBC_{SR} were 0.285 mm, and 0.012 mm, respectively. It was noticed that adopting PSHCC plates as a strengthening technique in this study significantly reduced the estimated shear crack width of the tested RCHBs compared to the un-strengthened beam (HBC_{NSR}). That relates to the adopted PSHCC plates' crack-arresting action, which delayed the crack propagation and improved the serviceability features of the strengthened RCHBs because of the fibers' bridging action and the strain-hardening phenomenon.

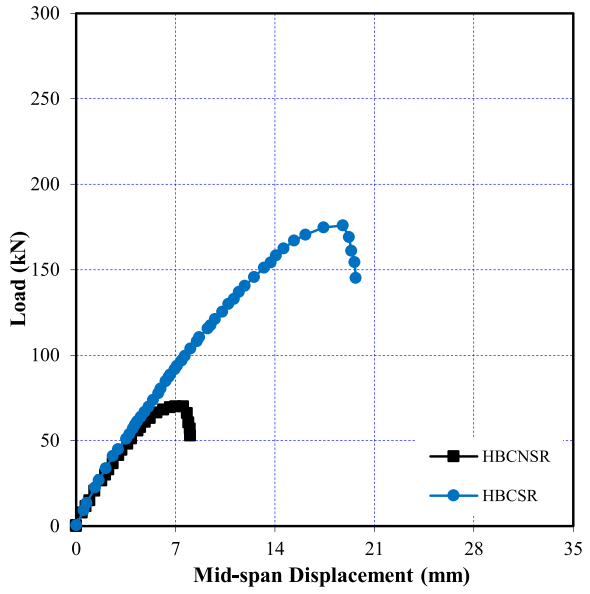
Based on the PSHCC plate's orientation, in comparison to adopting vertical PSHCC plates, using inclined PSHCC plates resulted in a reduction of crack widths. For instance, beam $HBS_{90\text{–}250\text{-}NSR}$ exhibited a 0.432 mm wide crack at a load level of about (133 kN) (see Fig. 11b), while beams $HBS_{45\text{–}250\text{-}NSR}$ and $HBS_{60\text{–}250\text{-}NSR}$, exhibited a crack width of 0.258 mm and 0.278 mm, respectively. This might be explained by the fact that the PSHCC plates were more effective at delimiting the developed cracks when their inclination angle was close to the direction of principal stresses. Furthermore, due to the higher PSHCC plate spacing, the crack arresting action of the PSHCC plate was reduced as depicted in Fig. 11c. Thus, at the same load 122 kN, the evaluated shear crack widths were wider for beam $HBS_{90\text{–}300\text{-}NSR}$ (0.471 mm) than those recorded for beams $HBS_{90\text{–}250\text{-}NSR}$ (0.293 mm) and $HBS_{90\text{–}200\text{-}NSR}$ (0.093 mm).

Referring to the position of the PSHCC plates relation to the inner web reinforcement, the applied load-crack width response of beams is depicted in Fig. 11d. It is clear that the crack widths of $HBS_{90\text{–}200\text{-}SR\text{-}Y1}$ (plates un-aligned with stirrup legs), $HBS_{90\text{–}200\text{-}SR\text{-}Y2}$ (plates aligned with stirrup legs), and $HBS_{57\text{–}200\text{-}SR\text{-}Y3}$ (plates inclined between stirrup legs) at the same load 170 kN were 0.067, 0.056 and 0.052 mm, respectively, compared to 0.292 mm for beam HBC_{SR}. These results clearly showed that the chosen strengthening technique (PSHCC plates) limited crack widths until the tested RCHBs' ultimate load was achieved, improving their serviceability properties.

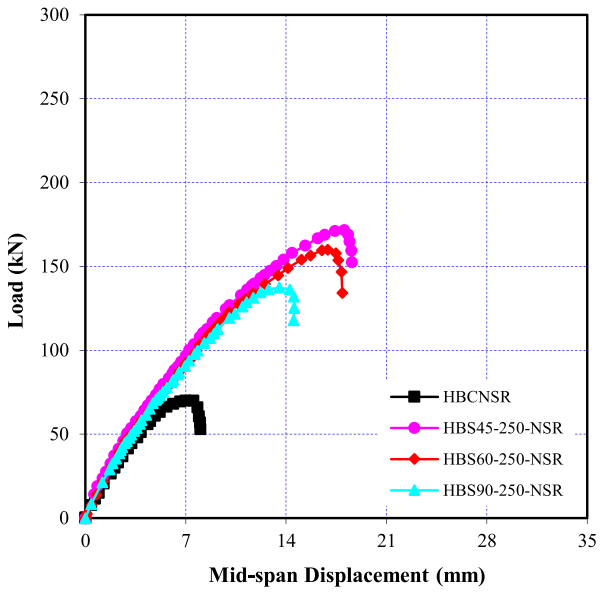
3.6. Strain analysis

As was previously described in Section 2.6, to measure the produced tensile strains, electrical resistance strain gauges were placed on the tension steel bars' surface. In order to determine the concrete strain in the compression zone, one electrical PI-shape (length of 100 mm) was positioned on each beam's concrete surface at the mid-span section (see Fig. 8). The load versus the concrete's compressive strain (left side) and the longitudinal reinforcement's tensile strain (right side) for all of the tested RC haunched beams are depicted in Fig. 12a to d, and Table 5 listed their maximum values.

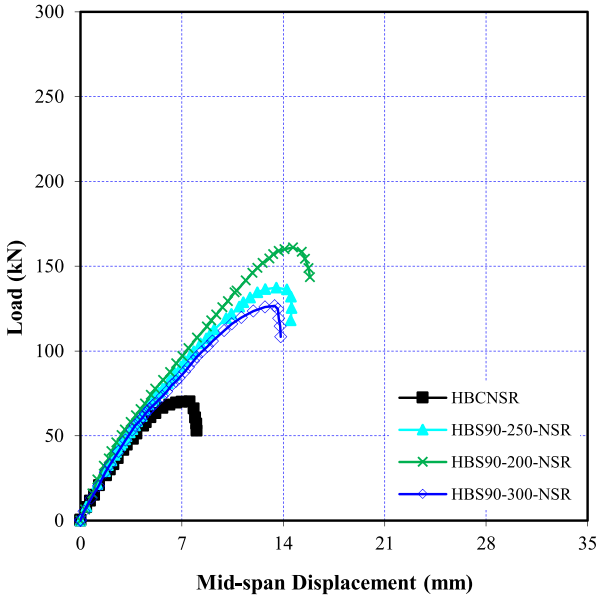
The strengthened RCHBs showed maximum tensile strains ranging from 1377 micro-strain ($HBS_{90\text{–}300\text{-}NSR}$) to 1956 micro-strain ($HBS_{57\text{–}200\text{-}SR\text{-}Y3}$). All failure modes were definitely shear failures since, as was to be anticipated, the maximum tensile strain of all tension reinforcements in all beams was significantly less than the yielding strain (ε_y = 2065 micro-strain). Furthermore, the concrete strain for each RC haunched beam was not more than the strain required to crush concrete (i.e., $\varepsilon_c < \varepsilon_{cu}$ = 3500 micro-strain). Maximum compressive strain in concrete exhibited that the PSHCC plates remarkably reduced the width of the major shear crack and altered the crack propagation, which significantly raised the compressive strain in concrete. Without web reinforcement in the shear region, RCHBs strengthened with PSHCC plates failed with compressive strain in concrete ranging from 1790 micro-strain ($HBS_{90\text{–}300\text{-}NSR}$) to 2487 micro-strain ($HBS_{90\text{–}200\text{-}NSR}$), as comparison to 1005 micro-strain for the control beam HBC_{NSR}. However, the highest compressive strains were achieved by the beams with web reinforcement in the strengthened shear zone among all tested beams. The maximum compressive strains in the concrete of ($HBS_{90\text{–}200\text{-}SR\text{-}Y1}$), ($HBS_{90\text{–}200\text{-}SR\text{-}Y2}$), and ($HBS_{57\text{–}200\text{-}SR\text{-}Y3}$) were 2757, 2588, and 2963 micro-strain,



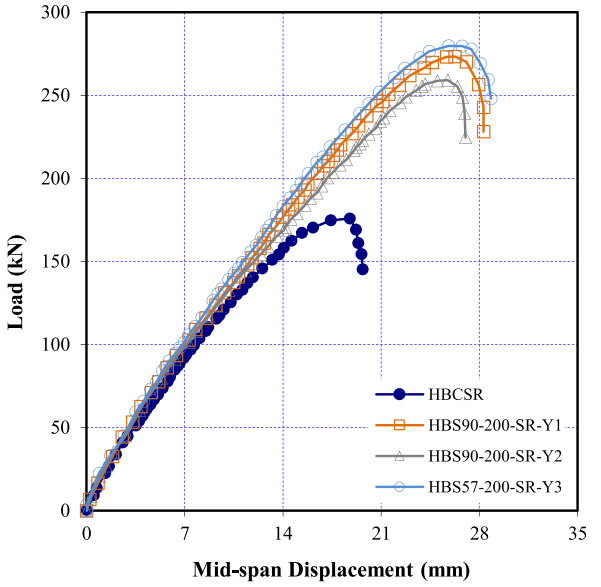
(a) Effect of shear reinforcement in the test region



(b) Effect of orientation angle of PSHCC plates



(c) Effect of spacing between the PSHCC plates



(d) Effect of PSHCC plates' position in relation to the inner stirrups

Fig. 10. Load-deflection curves for all tested RCHBs.

respectively compared to 1662 micro-strain for the beam HBC_{SR}.

It was observed that all strengthened RCHBs displayed higher values for both the compressive and tensile strains contrasted with the un-strengthened beam. This refers to the beneficial influence of the strengthening technique (PSHCC plates) in enhancing the ductility of the strengthened beams and postponing the brittle shear failure.

4. Estimation of the ultimate shear capacity formula for strengthened RCHBs

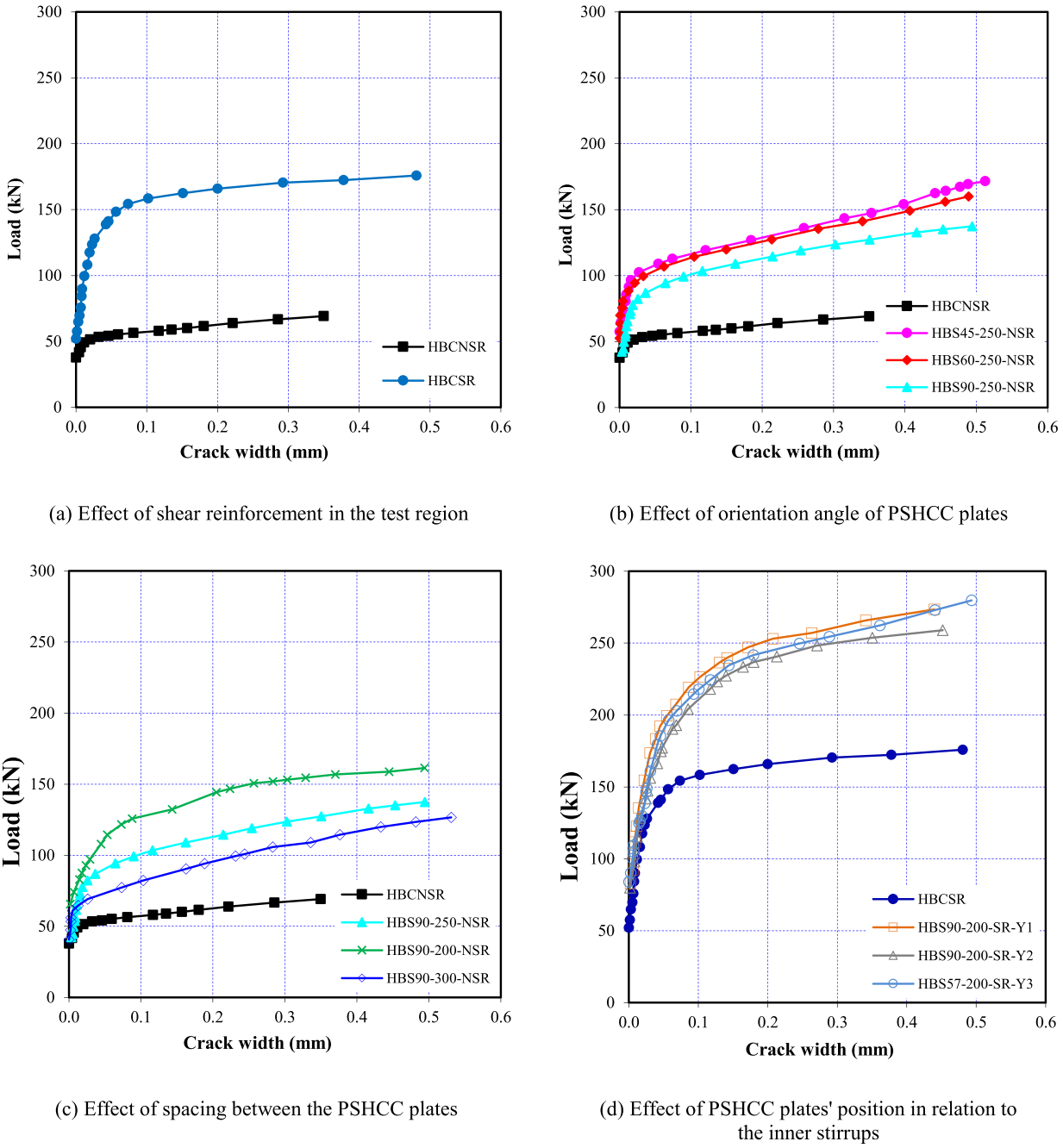
This section introduces an analytical model that is suggested for determining the ultimate shear capacity (V_{pro}) of RC haunched beams strengthened using PSHCC plates. The proposed shear capacity (V_{pro}) can be given in Eq. (1).

$$V_{pro} = V_c + V_s + V_{SHCC} \quad (1)$$

Where V_{pro} is the strengthened RCHBs' anticipated shear capacity; V_c is the shear force of concrete; V_s is the shear force of web reinforcement; and V_{SHCC} is the shear force resisted by the PSHCC plates.

4.1. The shear force of concrete (V_c)

According to Tena-Colunga et al. [40], the shear force of concrete (V_c) can be calculated in Eq. (2).



(a) Effect of shear reinforcement in the test region

(b) Effect of orientation angle of PSHCC plates

(c) Effect of spacing between the PSHCC plates

(d) Effect of PSHCC plates' position in relation to the inner stirrups

Fig. 11. Load-crack width curves for all tested RCHBs.

$$V_c = V_{pc} \pm V_{crk} \quad (2)$$

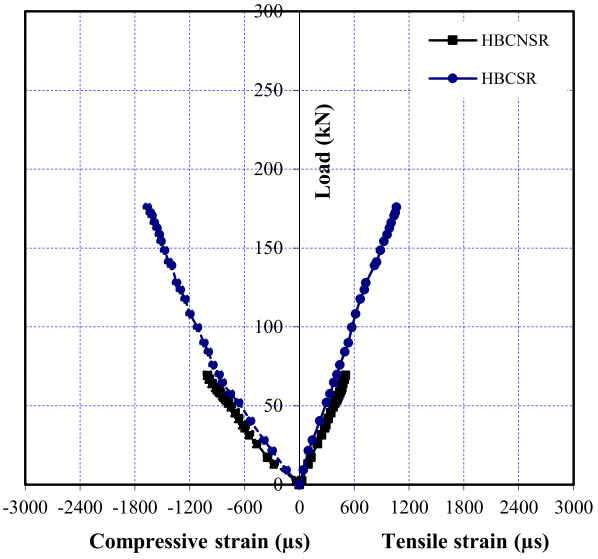
Where V_{pc} is the nominal concrete shear strength for a constant depth beam with the same cross section as that taken into consideration for a haunched beam, as given in Eq. (3) and V_{crk} is the shear force at the first diagonal tension crack, as given in Eq. (4) [41].

When the bending moment diagram rises in the same direction as the increase in haunch depth, V_{crk} uses a plus sign, and it uses a negative sign when the increase in the bending moment diagram increases in the opposite direction of the increase in haunch depth.

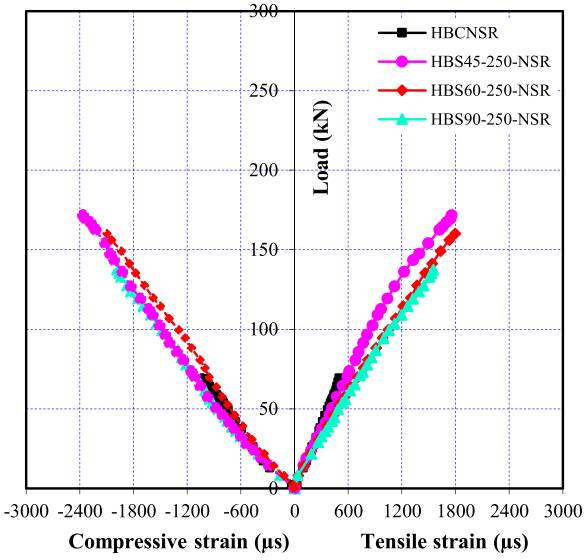
$$V_{pc} = \left(0.5\sqrt{f_c'} + 176\rho_w \frac{V_u d_{cr}}{M_u}\right) b d_{cr} \quad (3)$$

$$V_{crk} = \pm \frac{|M_{crk}|}{d_{\min}} \tan\alpha \quad (4)$$

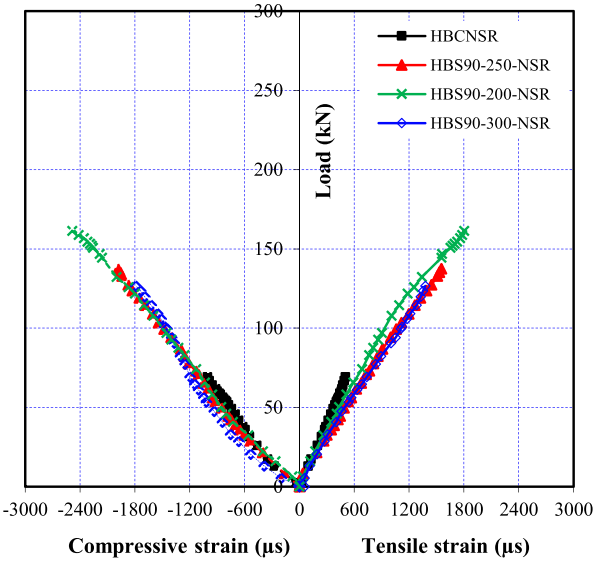
Where, f_c' is the cylinder concrete compressive strength after 28 days; b is the width of beam section; ρ_w is the longitudinal reinforcement ratio; d_{cr} is the effective equivalent depth at the critical haunched section as given in Eq. (5); M_u and V_u are respectively the ultimate moment and ultimate shear force applied at the critical section ($M_u = L_{cr} \times V_u$); L_{crit} is the position of shear plastic hinges as given in Eq. (6) that is measured from the supports and is associated with d_{cr} (see Fig. 13); M_{crk} is the bending moment at the first diagonal tension cracking as given in Eq. (7) [41]; α is the angle of the haunch's slope from the horizontal; d_{min} is the minimum effective depth for the haunched beam ($d_{min} = h_{min} - r$); h_{min} is



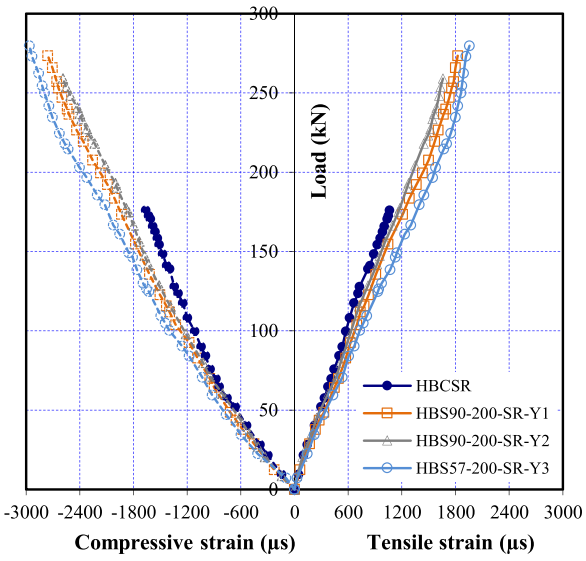
(a) Effect of shear reinforcement in the test region



(b) Effect of orientation angle of PSHCC plates



(c) Effect of spacing between the PSHCC plates



(d) Effect of PSHCC plates' position in relation to the inner stirrups

Fig. 12. Load versus compressive strain on the surface of the concrete and the longitudinal reinforcement's tensile strain.

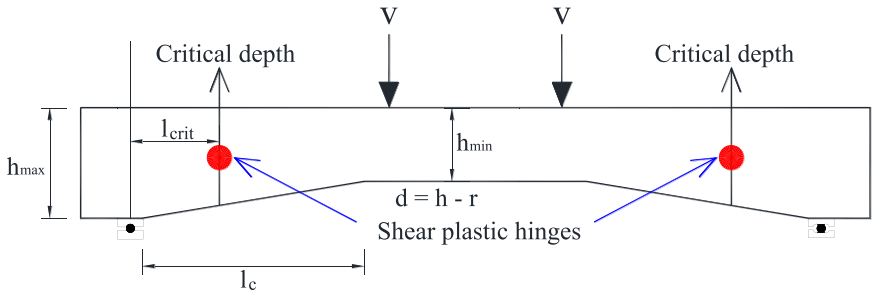


Fig. 13. Schematically location of plastic shear hinges [24].

the beam's depth at the central third; and r is the longitudinal reinforcement's concrete cover.

$$d_{cr} = d_{\min}(1 + 1.35\tan\alpha) \leq \left[\left(\frac{h_{\max}h_{\min} - (h_{\max})^2}{2l_c} + h_{\max} \right) - r \right] \quad (5)$$

$$L_{crit} = \frac{d_{\max} - d_{cr}}{\left(\frac{h_{\max} - h_{\min}}{l_c}\right)} \quad (6)$$

$$M_{crk} = 0.53\sqrt{f_c'}\, b \left(\frac{d_{cr}}{\sin\theta}\right)^2 \quad (7)$$

Where h_{max} is the depth at the beam ends; L_c is the length of the haunche; d_{max} is the maximum effective depth for the haunched beam; and θ is the major shear crack's angle from horizontal (θ = 45- α).

4.2. The shear force of web reinforcement (V_s)

Tena-Colunga et al. [40] suggested that it be assumed that the contribution of the web reinforcement in RC haunched beams is similar to the one for prismatic beams, that is, assuming cracking at 45° angle at one effective depth from the support, which can be obtained in Eq. (8).

$$V_s = \frac{A_v f_{yv} d_{cr}}{s_w \tan\theta} \quad (8)$$

Where A_v is the web reinforcement's area; f_{yv} is the web reinforcement's yield stress; and s_w is the web reinforcement's spacing.

4.3. The carrying capacity of PSHCC plates (V_{SHCC})

The shear strength resisted by the strengthening system (V_{SHCC}) is the sum of the shear strength provided by the sum of the SHCC material's tensile strengths as well as the embedded wire mesh steel in the PSHCC plates, as given in Eq. (9).

$$V_{SHCC} = \frac{(2A_{SHCC}f_{ty} + 2A_s f_{ys})d_{cr}}{s_p \tan\theta}(\sin\varphi + \cos\varphi) \quad (9)$$

Where, A_{SHCC} is the cross section area of one pre-cast SHCC plate($A_{SHCC} = w_p \times t_p$); w_p is the pre-cast plate's width (100 mm); t_p is the pre-cast plate's thickness (20 mm); f_{ty} is tensile yield strength of SHCC, which is regarded as being equivalent to the first cracking strength of SHCC (4.1 MPa) according to the Japan Society of Civil Engineers recommendations (JSCE) [44]; A_s is the total nominal area of embedded wire mesh steel in the pre-cast SHCC plate per one plate; f_{ys} is the tensile yield stress of the used embedded wire mesh steel (235 MPa); s_p is the longitudinal spacing between the centerlines of plates; φ is the plate's inclination angle with horizontal.

4.4. Verification of the proposed analytical model against the experimental results

Table 6 compares the experimental shear capacity (V_{exp}) and those deduced from the suggested shear capacity (V_{pro}) to assure that the shear capacity equation (V_{pro}) is accurate. $V_{exp.}/V_{pro}$ ratio was reported to range between 1.01 and 1.14, with a coefficient of variation (COV) of roughly 3.6%. This finding reveals that the suggested model, with an average error of roughly 7.4%, can accurately forecast the load carrying capacities for all RCHBs strengthened using PSHCC plates.

5. Conclusion

In this research, the shear performance of RCHBs strengthened with PSHCC plates was experimentally investigated. Ten simply supported RCHBs with different parameters were investigated. Furthermore, the proposed analytical model was used to forecast the shear capacity (V_{pro}) of the strengthened haunched beams (RCHBs). Based on the test results in the current study, the following conclusions can be established:

- The chosen strengthening technique has significantly improved all strengthened RCHBs' shear carrying capacity without any sign of debonding between the substrate concrete and PSHCC plates. The increase in P_{max} ranged from 48.8% to 148.5% compared to the unstrengthened control beam.
- The application of PSHCC plates restricted the manifestation of shear cracks on the substrate RC haunched beam. This may be related to the utilized PSHCC plates' ability to arrest cracks as a result of the fiber's bridging impact which inserted into the SHCC material.
- Inclined PSHCC plates performed better than vertical plates, especially when they were placed perpendicular to the line that connected the locations of load and support. The recorded capacities of $HBS_{45\text{-}250\text{-}NSR}$ (171 kN) and $HBS_{60\text{-}250\text{-}NSR}$ (160 kN) were about 24.8% and 16.7% higher than those of $HBS_{90\text{-}250\text{-}NSR}$ (137 kN) having vertical plates, respectively.
- The gain in ultimate capacity increased as the spacing between the PSHCC plates was reduced. Hence, the 200 mm plate spacing produced the highest performance for the enhanced beams. This prevented the generated main shear crack from propagating by allowing more than one plate to cross it. As a result, the load capacity and diagonal crack width could be effectively improved.

Table 6
Validation of the experiment results with the proposed analytical model.

Beam I.D	$V_{exp} = P_{exp}/2$ (kN)	Equation proposed using an analytical model						
		V_{pc} (kN)	V_{crk} (kN)	V_c (kN)	V_s (kN)	V_{SHCC} (kN)	V_{pro} (kN)	V_{exp}/V_{pro}
HBC_{NSR}	35.00	61.48	-30.88	30.61	0.00	0.00	30.61	1.14
HBC_{SR}	87.00	61.48	-30.88	30.61	52.49	0.00	83.10	1.05
$HBS_{45\text{-}250\text{-}NSR}$	85.50	61.48	-30.88	30.61	0.00	47.51	78.12	1.09
$HBS_{60\text{-}250\text{-}NSR}$	80.00	61.48	-30.88	30.61	0.00	45.89	76.50	1.05
$HBS_{90\text{-}250\text{-}NSR}$	68.50	61.48	-30.88	30.61	0.00	33.57	64.18	1.07
$HBS_{90\text{-}200\text{-}NSR}$	81.50	61.48	-30.88	30.61	0.00	41.97	72.58	1.12
$HBS_{90\text{-}300\text{-}NSR}$	63.50	61.48	-30.88	30.61	0.00	27.98	58.59	1.08
$HBS_{90\text{-}200\text{-}SR\text{-}Y1}$	136.50	61.48	-30.88	30.61	52.49	41.97	125.07	1.09
$HBS_{90\text{-}200\text{-}SR\text{-}Y2}$	129.50	61.48	-30.88	30.61	52.49	41.97	125.07	1.04
$HBS_{57\text{-}200\text{-}SR\text{-}Y3}$	141.00	61.48	-30.88	30.61	52.49	56.51	139.61	1.01
Average								1.074
Standard deviation								0.038
Coefficient of variation								0.036

V_{exp} is the experimental ultimate shear capacity; P_{exp} is the experimental ultimate load; V_c is the shear force of concrete; V_{crk} is the first diagonal tension cracking's shear force; V_{pc} is the nominal concrete shear strength; V_s is the web reinforcement's shear force; V_{SHCC} is the PSHCC plates' shear resistance; V_{pro} is the strengthened RCHBs' proposed shear capacity

- Among all strengthened beams, RCHBs beams with web reinforcement in the critical shear zone and strengthened using PSHCC plates achieved the maximum shear load. Moreover, the un-aligned PSHCC plates with inner web reinforcement also performed better than the aligned ones. This was due to the increase in the contact shear area which has been extended to cover most of the critical shear zone area using inner stirrups and the PSHCC plates at different locations rather than confinement of the same points internally by shear reinforcements and externally by the PSHCC plates.
- The proposed analytical model was used to anticipate the load capacities (V_{pro}) of the strengthened RC haunched beams using PSHCC plates. The results of the current experimental work were found to be in good accord with the model's prediction.

CRediT authorship contribution statement

Mohammed Fathy Sheta: Conceptualization, Data curation, Formal analysis, Investigation, Methodology, Resources, Writing – original draft, Writing – review & editing. **Ahmed M. Atta:** Conceptualization, Supervision. **Nesreen Kassem:** Conceptualization, Supervision. **Mahmoud A. Abdel-Aziz:** Conceptualization, Data curation, Formal analysis, Investigation, Methodology, Resources, Writing – original draft, Writing – review & editing.

Declaration of Competing Interest

The authors declare that they have no known competing financial interests or personal relationships that could have appeared to influence the work reported in this paper.

Data availability

Data will be made available on request.

References

[1] Aldahdooh MAA, Bunnori MN, Johari MA, Jamrah A, Alnuaimi A. Retrofitting of damaged reinforced concrete beams with a new green cementitious composites material. Compos Struct 2016;142:27–34. https://doi.org/10.1016/j.compstruct.2016.01.067.

[2] Al-Sulaimani GJ, Sharif A, Basunbul IA, Baluch MH, Ghaleb BN. Shear repair for reinforced concrete by fiberglass plate bonding. Struct J 1994;91:458–64.

[3] Hassan A, Baraghith AT, Atta AM, El-Shafiey TF. Retrofitting of shear-damaged RC T-beams using U-shaped SHCC jacket. Eng Struct 2021;245:112892. https://doi.org/10.1016/j.engstruct.2021.112892.

[4] Afefy HM, Baraghith AT, Hassan A, Abuzaid MK. Strengthening of shear-deficient RC beams using near surface embedded precast cement-based composite plates (PCBCPs). Eng Struct 2021;244:112765. https://doi.org/10.1016/j.engstruct.2021.112765.

[5] Baraghith AT, Mansour W, Behiry RN, Fayed S. Effectiveness of SHCC strips reinforced with glass fiber textile mesh layers for shear strengthening of RC beams: Experimental and numerical assessments. Constr Build Mater 2022;327:127036. https://doi.org/10.1016/j.conbuildmat.2022.127036.

[6] Khalil AEHA, Atta AM, Baraghith AT, Behiry RN, Soliman OE. Shear strengthening of concrete deep beams using pre-fabricated strain-hardening cementitious composite plates. Eng Struct 2023;278:115548. https://doi.org/10.1016/j.engstruct.2022.115548.

[7] ACI Committee 318 (2019). Building Code Requirements for Structural Concrete (ACI 318–19) and Commentary (ACI 318R-19). American Concrete Institute, Farmington Hills, MI, 519 ppfv.

[8] Tena A, Hernández O. Reinforced concrete haunched beams deficient in shear rehabilitated with jacketing of mortar and welded wire mesh. Bol Técnico 2009;47(2):37–56.

[9] Aziz, Aziz AH, Hassan HF, Razzaq FMA. Experimental study on shear behavior of reinforced self-compacted concrete tapered beams. Civ Environ Res 2016;8(8):11–22 (www.iiste.org).

[10] Al-Attar TS, Abdulqader SS, Ibrahim SK. Behavior of tapered self-compacting reinforced concrete beams strengthened by CFRP. Eng Technol J 2017;35(3):197–203. https://doi.org/10.30684/etj.35.3A.3.

[11] Al-Karkhi H, Aziz A. Shear strengthening of reinforced self-compacted concrete hammer head beams using warped CFRP strips: Experimental and theoretical study. Jordan J Civ Eng 2018;12(4).

[12] Al Jawahery MS, Gulsan ME, Albegmprli HM, Mansoori IAH, Cevik A. Experimental investigation of rehabilitated RC haunched beams via CFRP with 3D-FE modeling analysis. Eng Struct 2019;196:109301. https://doi.org/10.1016/j.engstruct.2019.109301.

[13] Tena-Colunga A, Hernandez-Marquez O, Archundia-Aranda HI. Strengthening of reinforced concrete prismatic and haunched beams using light jacketing. J Build Eng 2020;32:101757. https://doi.org/10.1016/j.jobe.2020.101757.

[14] Wakjira, Tena-Colunga A, Hernandez-Marquez O, Archundia-Aranda HI. Strengthening of reinforced concrete prismatic and haunched beams using light jacketing. J Build Eng 2020;32:101757. https://doi.org/10.1016/j.compositesb.2019.03.004.

[15] Naaman AE, Reinhardt HW. Characterization of high-performance fiber reinforced cement composites-HPFRCC. High Perform Fiber Reinf Cem Compos 2004;Vol. 2:1–24. https://doi.org/10.1201/9781482271676-8.

[16] Zhu JX, Xu LY, Huang BT, Weng KF, Dai JG. Recent developments in Engineered/Strain-Hardening Cementitious Composites (ECC/SHCC) with high and ultra-high strength. Constr Build Mater 2022;342:127956. https://doi.org/10.1016/j.conbuildmat.2022.127956.

[17] Choi JI, Song KI, Song JK, Lee BY. Composite properties of high-strength polyethylene fiber-reinforced cement and cementless composites. Compos Struct 2016;138:116–21. https://doi.org/10.1016/j.compstruct.2015.11.046.

[18] Afefy HM, Fawzy TM. Strengthening of RC one-way slabs including cut-out using different techniques. Eng Struct 2013;57:23–36. https://doi.org/10.1016/j.engstruct.2013.09.013.

[19] Afefy HM, Baraghith AT, Mahmoud MH. Retrofitting of defected reinforced-concrete cantilever slabs using different techniques. Mag Concr Res 2020;72(14):703–19. https://doi.org/10.1680/jmacr.18.00340.

[20] Afefy HM, Kassem NM, and, Mahmoud MH. Retrofitting of faulty reinforced concrete frame structures using two strengthening techniques. Mag Concr Res 2016;71(6):309–24. https://doi.org/10.1680/jmacr.17.00441.

[21] Li VC. From micromechanics to structural engineering-the design of cementitious composites for civil engineering applications. JSCE J Struct Mech Eq Eng 1993;10(2):3748. https://www.researchgate.net/publication/239060331.

[22] Li VC, Wang S, Wu C. Tensile strain-hardening behavior of polyvinyl alcohol engineered cementitious composite (PVA-ECC). Acids Mater J 2001;98(6):483–92. https://www.researchgate.net/publication/279888212.

[23] Li VC, Kanda T. Engineered cementitious composites for structural applications. J Mater Civ Eng 1998;10(2):66–79. http://worldcat.org/issn/08991561.

[24] Figueiredo TCS, Curosu I, Gonzales GL, Hering M, de Andrade Silva F, Curbach M, Mechtcherine V. Mechanical behavior of strain-hardening cement-based composites (SHCC) subjected to torsional loading and to combined torsional and axial loading. Mater Des 2021;198:109371. https://doi.org/10.1016/j.matdes.2020.109371.

[25] Li VC. Damage tolerant ECC for integrity of structures under extreme loads. Struct Congr 2009: Don't Mess Struct Eng: Expand Our Role 2009:1–10. https://doi.org/10.1061/41031(341)242.

[26] Li VC. High performance fiber reinforced cementitious composites as durable material for concrete structure repair/Faser verstärkte, Zement gebundene, zusammen gesetzte Hochleistungswerkstoffe für das dauerhafte Instandsetzen von Betontragwerken. Restor Build Monum 2004;10(2):163–80. https://doi.org/10.1515/rbm-2004-5844.

[27] Kim YY, Fischer G, Li VC. Performance of bridge deck link slabs designed with ductile engineered cementitious composite. Struct J 2004;101(6):792–801. https://doi.org/10.14359/13454.

[28] Kendall A, Keoleian GA, Lepech MD. Materials design for sustainability through life cycle modeling of engineered cementitious composites. Mater Struct 2008;41(6):1117–31. https://doi.org/10.1617/s11527-007-9310-5.

[29] Lepech MD, Li VC. Application of ECC for bridge deck link slabs. Mater Struct 2009;42(9):1185–95. https://doi.org/10.1617/s11527-009-9544-5.

[30] Jin Q, Faraldos M, Bahamonde A, Zaribaf BH, Kurtis KE. Titania and silica nanoparticle-modified coatings for cementitious materials. Spec Publ 2019;335:97–111. https://doi.org/10.14359/51720218.

[31] Hussein M, Kunieda M, Nakamura H. Strength and ductility of RC beams strengthened with steel-reinforced strain hardening cementitious composites. Cem Concr Compos 2012;34(9):1061–6. https://doi.org/10.1016/j.cemconcomp.2012.06.004.

[32] Khalil AEH, Etman E, Atta A, Essam M. Behavior of RC beams strengthened with strain hardening cementitious composites (SHCC) subjected to monotonic and repeated loads. Eng Struct 2017;140:151–63. https://doi.org/10.1016/j.engstruct.2017.02.049.

[33] Zhang Y, Zhang S, Deng M. Four-point bending tests of ECC: Mechanical response and toughness evaluation. Case Stud Constr Mater 2022;17:e01573. https://doi.org/10.1016/j.cscm.2022.e01573.

[34] Zhang Y, Zhang S, Li T, Deng M. Cyclic response and shear mechanisms of RC short walls strengthened with engineered cementitious composites thin layers. Arch Civ Mech Eng 2023;23(3):148. https://doi.org/10.1007/s43452-023-00683-x.

[35] NTCC-2004, Normas Tecnicas Complementarias para Diseno y Construccion de Estructuras de Concreto. Gaceta Oficial del Distrito Federal. Mexico; October, 2004 [in Spanish]. http://10.10.254.13/prontuario/vigente/743.htm.

[36] Wang CK, Salmon CG. Reinforced Concrete Design. 3rd ed..,. New York (USA): Harper and Row Publishers,; 1979 (www.wiley.com/college/wang).

[37] MacLeod IA, Houmsi A. Shear strength of haunched beams without shear reinforcement. Acids Struct J 1996;91(1):79–89 (http://www.concrete.org/PUBS/JOURNALS/SJHOME.ASP).

[38] Tena-Colunga A. Stiffness formulation for nonprismatic beam elements. ASCE J Struct Eng 1996;122(12):1484–9. https://doi.org/10.1061/(ASCE)07339445(1996)122:12(1484).

[39] Debaiky SY, El-Niema EI. Behavior and strength of reinforced concrete haunched beams in shear. Acids J 1982;79(3):184–94.
[40] Tena-Colunga A, Archundia-Aranda HI, and, González-Cuevas OM. Behavior of reinforced concrete haunched beams subjected to static shear loading. Eng Struct 2008;30:478–92. https://doi.org/10.1016/j.engstruct.2007.04.017.
[41] Godínez-Domínguez EA, Tena-Colunga A, and, Juárez-Luna J. Nonlinear finite element modeling of reinforced concrete haunched beams designed to develop a shear failure. Eng Struct 2015;105:99–122. https://doi.org/10.1016/j.engstruct.2015.09.023.
[42] ASTM C39/C39M-21, Standard Test Method for Compressive Strength of Cylindrical Concrete Specimens, ASTM International, 2021, www.astm.org.
[43] ASTM E8/E8M-22. Standard Test Methods for Tension Testing of Metallic Materials. Annual Book of ASTM Standards: West Conshohocken, PA, USA; 2022.
[44] Yokota H, Rokugo K, Sakata N. JSCE recommendations for design and construction of high performance fiber reinforced cement composite with multiple fine cracks. High Performance Fiber Reinforced Cement Composites. Tokyo, Japan: Springer,; 2008.
[45] Moreno-Martínez J, Meli R. Experimental study on the structural behavior of concrete dapped-end beams. Eng Struct 2014 2014;75:152–63. https://doi.org/10.1016/j.engstruct.2014.05.051.
[46] Khalil AEH, Etman E, Atta A, Baraghith A, Behiry R. The Effective Width in Shear Design of Wide-shallow Beams: A Comparative Study. KSCE J Civ Eng 2019;23(4):1670–81. https://doi.org/10.1007/s12205-019-0830-7.
[47] Younis A, Ebead U, Shrestha KC. Different FRCM systems for shear-strengthening of reinforced concrete beams. Constr Build Mater 2017;153:514–26. https://doi.org/10.1016/j.conbuildmat.2017.07.132.

Update

Engineering Structures

Volume 309, Issue , 15 June 2024, Page

DOI: https://doi.org/10.1016/j.engstruct.2024.118060

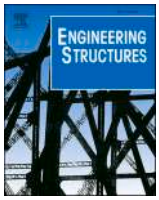
Engineering Structures 309 (2024) 118060



Contents lists available at ScienceDirect

Engineering Structures

journal homepage: www.elsevier.com/locate/engstruct





Corrigendum to "Ability of pre-cast strain-hardening cementitious composite plates to enhance the shear performance of RC haunched beams" [Eng Struct 307 (2024) 117891]

Mohammed F. Sheta [a,*], Ahmed M. Atta [b], Nesreen Kassem [b], Mahmoud A. Abdel-Aziz [b]

[a] Demonstrator, Structural Engineering Dept., Faculty of Engineering, Tanta University, Tanta, Egypt
[b] Structural Engineering Dept., Faculty of Engineering, Tanta University, Tanta, Egypt

The authors regret that the co-author's affiliation and designation in the published article is incorrect. The current designation of Mahmoud A. Abdel-Aziz, who is listed as the fourth author, is mentioned as "Assistant Professor" instead of "Associate Professor" to accurately reflect his current academic position.

The authors would like to apologise for any inconvenience caused.

DOI of original article: https://doi.org/10.1016/j.engstruct.2024.117891.
* Corresponding author.
E-mail address: Mohammed.Sheta@f-eng.tanta.edu.eg (M.F. Sheta).

https://doi.org/10.1016/j.engstruct.2024.118060

Available online 25 April 2024
0141-0296/© 2024 Elsevier Ltd. All rights reserved.